Mon. Not. R. Astron. Soc. **000**, 1–28 (2007) Printed 18 April 2008 (MN LaTeX style file v2.2)

arXiv:0804.2951v1 [astro-ph] 18 Apr 2008

A Monte Carlo simulation of the intergalactic absorption and the detectability of the Lyman continuum from distant galaxies

Akio K. Inoue[1]* and Ikuru Iwata[2]

[1] *College of General Education, Osaka Sangyo University, 3-1-1, Nakagaito, Daito, Osaka 574-8530, Japan*

[2] *Okayama Astrophysical Observatory, National Astronomical Observatory of Japan, Kamogata, Okayama 719-0232, Japan*

Accepted Received; in original form

ABSTRACT

We have made a Monte Carlo simulation of the intergalactic absorption in order to model the Lyman continuum absorption, which is required to estimate the escape fraction of the Lyman continuum from distant galaxies. To input into the simulation, we derive an empirical distribution function of the intergalactic absorbers which reproduces recent observational statistics of the Lyman α forest, Lyman limit systems (LLSs), and damped Lyman α systems (DLAs) simultaneously. In particular, we assume a common functional form of the number evolution along the redshift for all types of absorbers. The Lyman series transmissions in our simulation reproduce the observed redshift evolution of the transmissions excellently, and the Lyman continuum transmission also agrees with an observed estimation which is still quite rare in the literature. The probability distribution of the Lyman α opacity in our simulation is log-normal with a tail towards a large opacity. This tail is produced by DLAs. The probability distribution of the Lyman continuum opacity in our simulation also show a broad tail towards a large opacity. This tail is produced by LLSs. Because of the rarity of LLSs, we have a chance to have a clean line of sight in the Lyman continuum even for $z \sim 4$ with a probability of about 20%. Our simulation expects a good correlation between the Lyman continuum opacity and the Lyman α opacity, which may be useful to estimate the former from the latter for an individual line of sight.

Key words: cosmology: observation — intergalactic medium

1 INTRODUCTION

Neutral hydrogen remaining in the intergalactic medium (IGM) absorbs the radiation from distant sources (e.g., Gunn & Peterson 1965). This intergalactic absorption seems to be caused by numerous discrete systems, which are called absorbers in this paper, on the line of sight. The absorbers probably consist of various types of objects: the outer edge of galaxies, halo gas, diffuse medium in the intergalactic space, etc. They probably connect with each other and form the "cosmic web" (e.g., Rauch 1998).

Because of such clumpy nature of the IGM, the intergalactic absorption fluctuates among the lines of sight. Thus, we cannot predict the amount of the absorption for a certain line of sight. However, we can predict a mean amount of the absorption with its standard deviation for many lines of sight in a statistical sense (e.g., Møller & Jakobsen 1990; Giallongo & Cristiani 1990; Zuo 1993; Madau 1995). Bershady et al. (1999) showed that a Monte Carlo simulation is very powerful to discuss not only the mean absorption but also the dispersion correctly. Here we present such a simulation. Because many observational results of the IGM absorbers have been published since 1999, we update the absorbers' statistics to be input into the simulation.

Recently, Meiksin (2006) presented a new mean curve of the intergalactic absorption based on the density distribution produced by a cosmological simulation. However, he discussed mean transmission only. Tepper-García & Fritze (2008) have done a Monte Carlo simulation and discuss the distribution of the absorption amount. However, they concentrate on only Lyman α absorption. In this paper, we will examine the stochastic nature not only of the Lyman series absorption but also of the Lyman continuum one.

This is motivated by the recent observational attempts for determining the escape fraction of the Lyman continuum, especially the hydrogen ionising photons, from distant galaxies (e.g., Steidel et al. 2001; Giallongo et al. 2002; Malkan, Webb, & Konopackey 2003; Inoue et al. 2005; Shapley et al. 2006; Siana et al. 2007). In the process towards the escape fraction, we need a correction of the intergalactic absorption for the Lyman continuum of the distant galaxies. Since the Lyman continuum absorption by the IGM has not been measured well observationally, a model predicting the absorption amount of the Lyman continuum is required.

⋆ E-mail: akinoue@las.osaka-sandai.ac.jp (AKI)

The effective optical depth through a clumpy IGM for the frequency $\nu_{\rm S}$ in the rest-frame of a source at the redshift $z_{\rm S}$ is (e.g., Paresce et al. 1980)

$$\tau_{\rm eff}(\nu_{\rm S}, z_{\rm S}) = \int_0^{z_{\rm S}} dz \int_{N_{\rm l}}^{N_{\rm u}} dN_{\rm HI} \frac{\partial^2 \mathcal{N}}{\partial z \partial N_{\rm HI}} (1 - e^{-\tau_{\rm cl}}) \,, \tag{1}$$

where $\partial^2\mathcal{N}/\partial z\partial N_{\rm HI}$ is the number of absorbers along the line of sight per unit redshift z interval and per unit HI column density $N_{\rm HI}$ interval, and $\tau_{\rm cl} = \sigma_{\rm HI}(\nu_{\rm S}(1+z)/(1+z_{\rm S}))N_{\rm HI}$ is the optical depth of an absorber with $N_{\rm HI}$ at z, with being the HI cross section $\sigma_{\rm HI}(\nu)$ at the frequency ν in the absorber's rest-frame. If we assume the column density distribution of the absorbers as a power-law with an index $-\beta$ independent of the redshift, which is well found in observations (e.g., Tytler 1987), we have

$$N_{\rm HI} \frac{\partial \tau_{\rm eff}}{\partial N_{\rm HI}} \propto N_{\rm HI}^{1-\beta} (1 - e^{-\tau_{\rm cl}}) \propto \begin{cases} N_{\rm HI}^{2-\beta} & (\tau_{\rm cl} \ll 1) \\ N_{\rm HI}^{1-\beta} & (\tau_{\rm cl} \gg 1) \end{cases} . \tag{2}$$

Since observations show $\beta \approx 1.5$ (e.g., Tytler 1987), the maximum contribution to $\tau_{\rm eff}$ is made by absorbers with $\tau_{\rm cl} \sim 1$ (e.g., Møller & Jakobsen 1990; Meiksin 2006). Thus, the absorption of the Lyman continuum is mainly caused by the Lyman limit systems (LLSs) with $N_{\rm HI} \sim 10^{17}$ cm^{-2}, not by the Lyman α forest (LAF) with $N_{\rm HI} \sim 10^{13}$ cm^{-3}. Therefore, we take a great care of the treatment of LLSs in order to properly compute the Lyman continuum absorption by the IGM. Moreover, the Lyman continuum absorption should be very stochastic because LLSs are relatively rare. Therefore, we also need to model the dispersion of the absorption correctly.

Previous works about the intergalactic absorption assumed different number evolutions along the redshift for the LAF and LLSs. Madau (1995) assumed $d\mathcal{N}/dz \propto (1+z)^{2.46}$ for the LAF (Murdoch et al. 1986) and $d\mathcal{N}/dz \propto (1+z)^{0.68}$ for LLSs (Sargent et al. 1989). Bershady et al. (1999) assumed a different set of the LAF number evolution and the same LLS evolution as Madau (1995) (see also Tepper-García & Fritze 2008). Meiksin (2006) assumed the number evolution extracted from a cosmological simulation for the LAF and $d\mathcal{N}/dz \propto (1+z)^{1.5}$ for LLSs (Stengler-Larrea et al. 1995). However, Inoue et al. (2005) showed in their appendix that recent LLSs observations reported by Péroux et al. (2003) can be reproduced by a common number evolution function for both types of absorbers. We take this common function scenario in this paper because of its simplicity.

The rest of this paper consists of 5 sections; in section 2, we present an empirical distribution function of the intergalactic absorbers and show that the function reproduces all the observational data simultaneously. In section 3, we describe the procedure of our Monte

Carlo simulation. In section 4, we describe the method for calculating the IGM transmission, compare our transmission model with others, show that our model reproduces the observed Lyman series transmissions very well, predict the Lyman continuum transmission, discuss the distribution functions of the intergalactic opacities of the Lyman continuum as well as Lyman α line, and present a method for estimating the Lyman continuum opacity from the Lyman α one. In section 5, we discuss the detectability of the Lyman continuum from distant galaxies with our Monte Carlo results. The final section is devoted to our conclusions.

2 DISTRIBUTION FUNCTION OF INTERGALACTIC ABSORBERS

In this section, we present an empirical distribution function of the intergalactic absorbers which is input into the Monte Carlo simulation in the later sections. We consider a functional form with several parameters which are determined so as to reproduce the observed redshift, column density, and Doppler parameter distributions of the intergalactic absorbers. Especially, we assume a common number evolution function along the redshift for all types of absorbers.

An absorber have three physical quantities characterising itself: redshift z, HI column density $N_{\rm HI}$, and Doppler parameter b. Here, we assume that these three quantities are independent of each other. This is just for simplicity although a slight correlation between $N_{\rm HI}$ and b has found (e.g., Kim et al. 2001). Then, we express the number of absorbers per unit volume of the three parameters' space as

$$\frac{\partial^3 \mathcal{N}}{\partial z \partial N_{\rm HI} \partial b} = f(z) g(N_{\rm HI}) h(b)\,. \tag{3}$$

Note that we have assumed a common functional form of the number evolution along the redshift for all types of absorbers as $f(z)$. In the following, we determine the functional forms of $f(z)$, $g(N_{\rm HI})$, and $h(b)$ so as to reproduce the observed distribution functions. Since the observed statistics of absorbers are not very tight yet, we do it by visual inspection instead of doing it by a rigorous way like a likelihood method.

Figure 1 shows the column density distribution. The vertical axis is the number of absorbers per unit column density and per unit "absorption distance" which was introduced to remove the effect of the Hubble expansion (Bahcall & Peebles 1969). While Tytler (1987) proposed a single power-law for the column density distribution, the recent data seems a double power-law with a break at $\sim 10^{17}$ cm^{-2} as found in Figure 1. Prochaska et al. (2005) also suggest a similar break around 10^{17} cm^{-2}. For the highest column density, however,

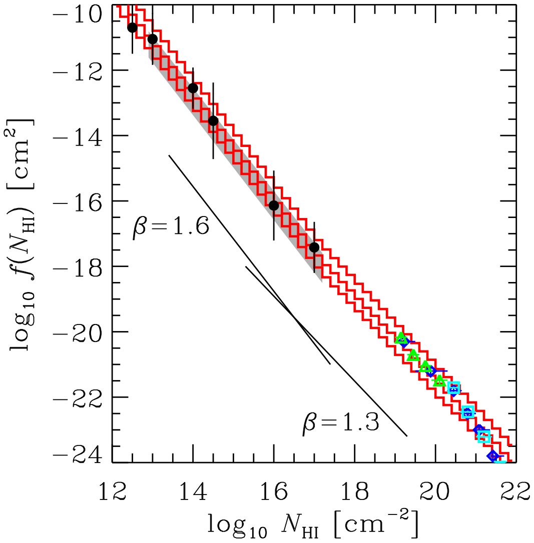

Figure 1. Number of the intergalactic absorbers per unit column density per unit "absorption distance" along an average line of sight as a function of the column density. The shaded area is the observed range of the Lyman α forest (LAF) at $z_{\rm abs} = 0.5$–1.9 by Janknecht et al. (2006). The filled circles are the data of the LAF at $z_{\rm abs} = 1.5$–4.0 based on Kim et al. (2002). The diamonds, triangles, and squares are the observed data of sub-damped Lyman α systems (sub-DLAs) and damped Lyman α systems (DLAs) by Peroux et al. (2005; $z_{\rm abs} = 1.8$–5.0), O'Meara et al. (2007; $z_{\rm abs} = 1.8$–4.2), and Prochaska et al. (2005; $z_{\rm abs} = 2.2$–5.5), respectively. All the data are scaled for a flat Λ cosmology with $\Omega_\Lambda = 0.7$. The histograms are the column density distributions of absorbers generated by our Monte Carlo simulation: the absorber's redshift $z_{\rm abs} = 0$–2 (bottom), 2–4 (middle), and 4–6 (top). The vertical shifts of the histograms are the result of the number density evolution along the redshift. The two solid lines are for the reference of the power-law index.

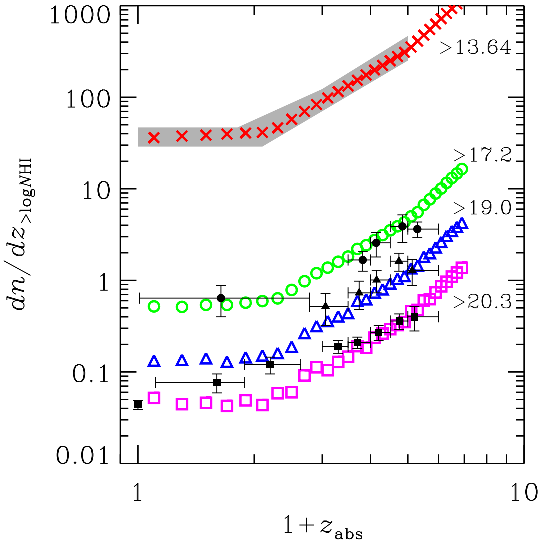

Figure 2. Number of the intergalactic absorbers per unit redshift along an average line of sight as a function of the absorbers' redshift. The shaded area is the observed range for absorbers with $\log_{10}(N_{\rm HI}/{\rm cm}^{-2}) > 13.6$ (LAF) taken from Weymann et al. (1998), Kim et al. (2001), and Janknecht et al. (2006). The filled circles, triangles, and squares are the observed data of absorbers with $\log_{10}(N_{\rm HI}/{\rm cm}^{-2}) > 17.2$ (LLS) taken from Peroux et al. (2005), > 19.0 (sub-DLA) taken from Peroux et al. (2005), and > 20.3 (DLA) taken from Rao et al. (2006), respectively. The number density evolutions of absorbers generated by our Monte Carlo simulation are shown by different symbols depending on the column density range: crosses ($\log_{10}(N_{\rm HI}/{\rm cm}^{-2}) > 13.6$), open circles ($\log_{10}(N_{\rm HI}/{\rm cm}^{-2}) > 17.2$), open triangles ($\log_{10}(N_{\rm HI}/{\rm cm}^{-2}) > 19.0$), and open squares ($\log_{10}(N_{\rm HI}/{\rm cm}^{-2}) > 20.3$). They excellently trace the assumed distribution functions of absorbers given in equations (3)–(6), but we see statistical fluctuations in large column density cases due to the small number of such absorbers.

there may be a more rapid decline of the number of absorbers, suggesting a Schechter like function for this column density range (Péroux et al. 2003; Prochaska et al. 2005). Here we adopt a double power-law for simplicity as

$$g(N_{\rm HI}) = B \begin{cases} \left(\frac{N_{\rm HI}}{N_{\rm c}}\right)^{-\beta_1} & (N_{\rm l} \leqslant N_{\rm HI} < N_{\rm c}) \\ \left(\frac{N_{\rm HI}}{N_{\rm c}}\right)^{-\beta_2} & (N_{\rm c} \leqslant N_{\rm HI} \leqslant N_{\rm u}) \end{cases} , \tag{4}$$

with $\beta_1 = 1.6$ and $\beta_2 = 1.3$ obtained by eye. The break column density $N_{\rm c}$ is assumed to be 1.6×10^{17} cm^{-2} which is the usual criterion for LLSs, i.e. the absorber with a column density larger than this value is optically thick for the Lyman limit photon. A physical explanation for this break, which gives more number of higher column density absorbers, is a self-shielding effect; the neutral fraction inside an optically thick absorber (i.e. LLSs) could be kept higher. The normalisation B is determined by $\int_{\rm N_l}^{N_{\rm u}} g(N_{\rm HI}) dN_{\rm HI} = 1$.

Figure 2 shows the number evolution along the redshift of the LAF, LLSs, sub-DLAs, and DLAs. The LAF number evolution (the shaded area) shows a break at $z \sim 1$ (Weymann et al. 1998). Davé et al. (1999) have explained that this break is due to a steep decline of the ionising background intensity from $z \sim 1$ to 0. Thus, we assume a break at $z \sim 1$ in the functional form of $f(z)$. On the other hand, Fan et al. (2006) suggest a steepening of the Lyman α opacity evolution at $z \gtrsim 4$, which means more absorbers than expected at high redshift. As done in Inoue et al. (2006), thus, we assume another break at $z \sim 4$ in $f(z)$. Therefore, we assume

$$f(z) = \mathcal{A} \begin{cases} \left(\frac{1+z}{1+z_1}\right)^{\gamma_1} & (0 < z \leqslant z_1) \\ \left(\frac{1+z}{1+z_1}\right)^{\gamma_2} & (z_1 < z \leqslant z_2) \\ \left(\frac{1+z_2}{1+z_1}\right)^{\gamma_2} \left(\frac{1+z}{1+z_2}\right)^{\gamma_3} & (z_2 < z) \end{cases} . \tag{5}$$

We adopt $z_1 = 1.2$, $\gamma_1 = 0.2$, and $\gamma_2 = 2.5$ which are determined by eye to fit the observed number evolutions along the redshift of the LAF in Figure 2. We also adopt the second break in $f(z)$ at $z_2 = 4.0$ with $\gamma_3 = 4.0$ to reproduce a rapid increase of the Lyman α opacity found by Fan et al. (2006). With these parameters, the observed number evolutions of all types of absorbers are reproduced simultaneously. Note that we have assumed $g(N_{\rm HI})$ to be a double power-law as equation (4). If we assumed $g(N_{\rm HI})$ to be a single power-law, we could not reproduce the number evolution functions of all types of absorbers simultaneously. The normalisation $\mathcal{A}$ is the total number of the IGM absorbers at $z = z_1$ with a column density $N_{\rm l} \leqslant N_{\rm HI} \leqslant N_{\rm u}$. We adopt $\mathcal{A} = 400$ with $N_{\rm l} = 10^{12}$ cm^{-2} and $N_{\rm u} = 10^{22}$ cm^{-2} to match with the observed number of the LAF in Figure 2.

Table 1. Parameters for the distribution function of intergalactic absorbers.

Parameters	Adopted value
γ_1	0.2
γ_2	2.5
γ_3	4.0
z_1	1.2
z_2	4.0
$\mathcal{A}$	400
$\log_{10}(N_{\rm l}/{\rm cm}^{-2})$	12.0
$\log_{10}(N_{\rm u}/{\rm cm}^{-2})$	22.0
$\log_{10}(N_{\rm c}/{\rm cm}^{-2})$	17.2
β_1	1.6
β_2	1.3
$b_\sigma/{\rm km\ s}^{-1}$	23.0

For the Doppler parameter distribution function $h(b)$, we assume the functional form with a single parameter b_σ suggested by Hui & Rutledge (1999):

$$h(b) = \frac{4{b_\sigma}^4}{b^5} e^{-{b_\sigma}^4/b^4} \,. \tag{6}$$

We adopt $b_\sigma = 23$ km s^{-1} based on the measurements by Janknecht et al. (2006). We note that $h(b)$ in equation (6) is already normalised as $\int_0^\infty h(b)db = 1$.

In Figures 1 and 2, we show comparisons of the empirical distribution functions presented in equations (4) and (5) with the observed functions. For our distribution functions, we show the results generated by our Monte Carlo simulation, whose procedures are described in the next section. We have confirmed that our Monte Carlo simulation reproduces the input distribution functions excellently. Figure 1 shows that our column density distribution $g(N_{\rm HI})$ is very consistent with the observations. Note that the vertical axis in the panel is not exactly same as $g(N_{\rm HI})$ but the column density distribution averaged over a redshift range (and divided by the "absorption distance"). Figure 2 shows that our redshift evolution $f(z)$ nicely reproduces the observed redshift evolution for all types of absorbers simultaneously. Note that the vertical axis in the panel is not exactly same as $f(z)$ but the number density of absorbers with column densities larger than a certain value. Although the disagreement of DLAs at $z \sim 1$ (but less than a factor of two) might suggest a redshift dependence of $g(N_{\rm HI})$, we avoid this complexity. The adopted values for the parameters are summarised in Table 1.

Figure 3 is the close-up of the number evolution of LLSs along the redshift. As described in section 1, we need to reproduce the observed number of LLSs for a rigid prediction of the Lyman continuum absorption by the IGM. Figure 3 ensures a good agreement between our model and observations by Péroux et al. (2005). On the other hand, the regression line

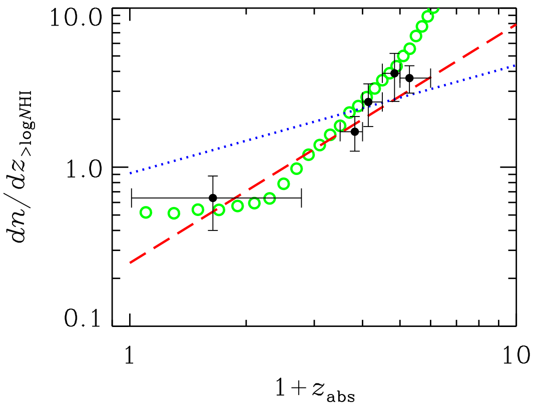

Figure 3. Number of LLSs per unit redshift along an average line of sight as a function of the LLSs' redshift. The filled circles are the recent observed data by Peroux et al. (2005). The open circles are our model. The dashed line is the regression line by Stengler-Larrea et al. (1995), which is assumed in Meiksin (2006). The dotted line is the regression line by Sargent et al. (1989), which is assumed in Madau (1995), Bershady et al. (1999), and Tepper-García & Fritze (2008).

suggested by Sargent et al. (1989) shown as the dotted line in Figure 3, which is assumed in Madau (1995), Bershady et al. (1999), and Tepper-García & Fritze (2008), does not agree well with the recent data. The dashed line in Figure 3 is the regression line suggested by Stengler-Larrea et al. (1995) which is assumed in Meiksin (2006). This case agrees with the recent data. However, in this case, we would need different functional forms of $f(z)$ for the LAF and for LLSs to fit all the data shown in Figure 2 simultaneously.

3 MONTE CARLO PROCEDURE

Based on the assumed distribution function described in the previous section, we generate a large number of absorbers along lines of sight by a Monte Carlo method. The random number generator used in this paper is the "Mersenne Twister" developed by Matsumoto & Nishimura (1998) which is a very fast random number generator with a very good statistical property. [1]

We assume the encounter of an absorber on a line of sight to be a Poisson process. In other words, we neglect the effect of clustering of absorbers although it has been already found (Ostriker, Bajtlik, & Duncan 1988). We should examine the effect in future. For a Poisson process, if we have an absorber at z, the probability encountering the next absorber at $z + \Delta z$ is

---

[1] The "Mersenne Twister" is proved to have the period of $2^{19937} - 1$ and the 623-dimension equidistribution property. Its C-code is public at http://www.math.sci.hiroshima-u.ac.jp/˜m-mat/MT/emt.html

$$p(\Delta z; z) = f(z) e^{-f(z)\Delta z} \,, \tag{7}$$

because the mean redshift interval of two absorbers at z is just the reciprocal of the redshift distribution function $f(z)$ of equation (5).

For a line of sight, we start from $z = 0$ and determine the redshift of the first absorber by drawing a random number based on equation (7), and we determine the column density and the Doppler parameter of this absorber by drawing other two random numbers based on $g(N_{\rm HI})$ and $h(b)$ of equations (4) and (6). We note that $g(N_{\rm HI})$ and $h(b)$ themselves are the probability distribution functions. Then, we determine the redshift, the column density, and the Doppler parameter of the next absorber likewise. These procedures are repeated until the absorber's redshift exceeds $z = 6$. Typically, we generate about 18,000 absorbers for one line of sight which depends on the lower limit of the column density $N_{\rm l}$. For a smaller $N_{\rm l}$, we need much more absorbers which is time-consuming. As shown in equation (2), absorbers with a column density less than $N_{\rm l} = 10^{12}$ cm^{-2} do not contribute to the opacity very much because their optical depths are much less than unity. We generate 10,000 lines of sight for enough statistics.

4 INTERGALACTIC TRANSMISSIONS

Based on the intergalactic absorbers along lines of sight generated by the Monte Carlo procedures described in the previous section, we calculate transmissions along the lines of sight.

Suppose an absorber with the redshift z, the column density $N_{\rm HI}$, and the Doppler parameter b. The optical depth of this absorber for the frequency ν in the absorber's rest-frame is

$$\tau(\nu) = N_{\rm HI} \left(\sigma_{\rm LC}(\nu) + \sum_i \sigma_i(\nu) \right) \,, \tag{8}$$

where $\sigma_{\rm LC}$ is the cross section for the Lyman continuum, and σ_i is the cross section of the i-th Lyman series line. The cross section for the Lyman continuum is approximated to

$$\sigma_{\rm LC}(\nu) = \sigma_{\rm LL} \left(\frac{\nu_{\rm LL}}{\nu} \right)^3 \qquad (\nu \geqslant \nu_{\rm LL}) \,, \tag{9}$$

where the cross section at the Lyman limit $\nu_{\rm LL}$ is $\sigma_{\rm LL} = 6.30 \times 10^{-18}$ cm^2 (Osterbrock 1989). When $\nu < \nu_{\rm LL}$, $\sigma_{\rm LC}(\nu) = 0$. The cross sections for the Lyman series lines are approximated to

$$\sigma_i(\nu) = \frac{\sqrt{\pi}e^2 f_i}{m_{\rm e} c \nu_{\rm D}} \phi_i(\nu)\,, \tag{10}$$

where $m_{\rm e}$ is the electron mass, e is the electron charge, c is the speed of light, f_i is the oscillator strength of the i-th line, $\nu_{\rm D} = \nu_i(b/c)$ is the Doppler width with the line centre frequency ν_i, and $\phi_i(\nu)$ is the line profile function which is calculated by an analytic approximation by Tepper-García (2006). The hydrogen atomic data of ν_i, f_i, and the damping constant Γ_i for the line profile up to 40-th line are taken from Wiese et al. (1966).

Since we consider only HI absorbers in this paper, we calculate the wavelength range not affected by helium: 700–1300 Å in the rest-frame of the source redshift. Note that we should consider wavelength enough longer than that of the Lyman α line (1216 Å) in order to treat a broad wing of damped Lyman α lines. We should also calculate transmissions with an enough high wavelength resolution. We have found experimentally that typical errors in transmissions within a wavelength range relative to those calculated with 0.01 Å resolution in the source rest-frame are 10% for 1 Å resolution and 1% for 0.1 Å resolution.[2] Thus, we have calculated all the results in this paper with 0.1 Å resolution in the source rest-frame.

4.1 Example and average transmissions

Figure 4 shows the IGM transmissions along an example line of sight. We find a lot of narrow absorption lines as the LAF. In the Lyman continuum region, we find several stepwise depressions caused by LLSs. For example, in the panel (b) ($z_{\rm S} = 3$ case), we find significant transmissions below the Lyman limit up to 864 Å at which a sharp depression appears because of a LLS at $z = 2.78$ which has $N_{\rm HI} = 6.5 \times 10^{17}$ cm^{-2}. This means that the Lyman continuum absorption by the IGM is very stochastic because it is controlled by the presence of relatively rare LLSs. This point is illustrated in Figure 5. If we do not have a LLS (or DLA) near the source, we can expect a significant transmission even far below the source Lyman limit (panel [a]). However, If we have such a LLS, the transmission is suddenly cut down at the corresponding wavelength (panel [b]).

On the other hand, such stochastic behaviour disappears in average transmissions shown in Figure 6, where we also compare our models with those by other authors. The solid line in each panel is our Monte Carlo model. We have averaged 10,000 lines of sight in each

---

[2] We should note that relative errors are larger for lower transmissions. For a very small transmission, say $\lesssim 10^{-3}$, the relative error becomes about 10% or more in some cases even with 0.1 Å resolution. Such cases appear in the Lyman continuum transmissions for the source redshift $z_{\rm S} \gtrsim 5$. However, the fraction of the cases is ~ 10%.

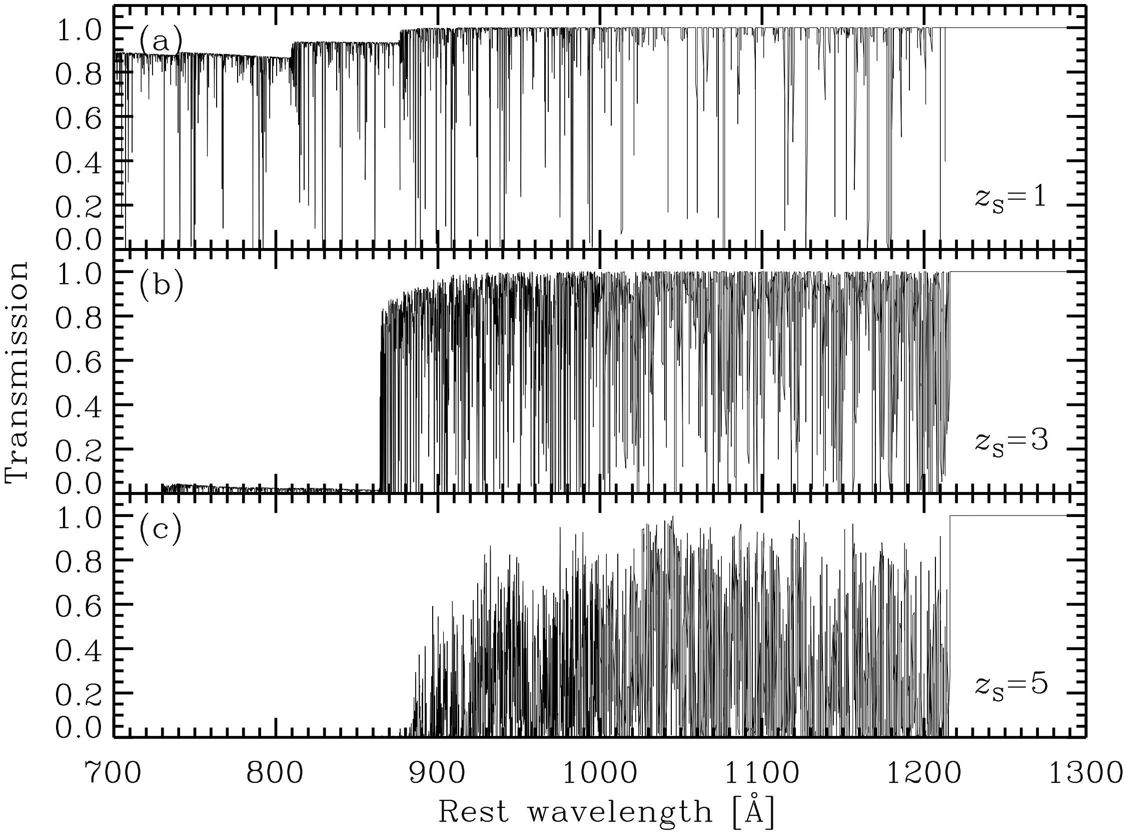

Figure 4. Examples of the IGM transmissions along a line of sight. The horizontal axis is the wavelength in the source rest-frame. The source redshifts are noted in the panels.

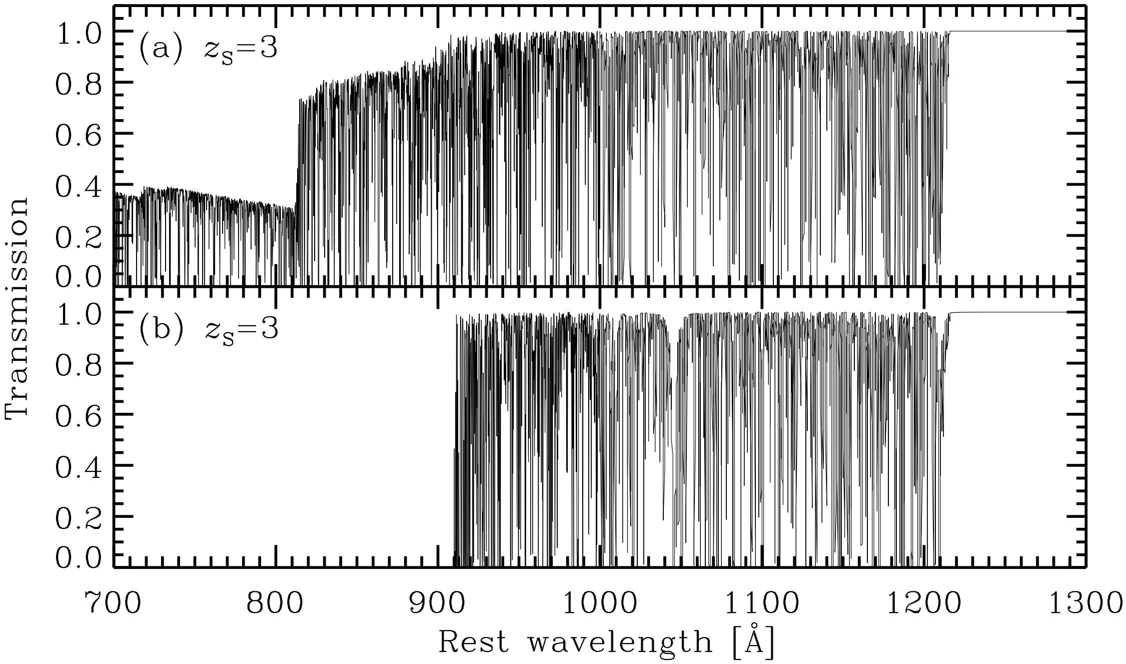

Figure 5. Example IGM transmissions of the source redshift $z_S = 3$ for different lines of sight.

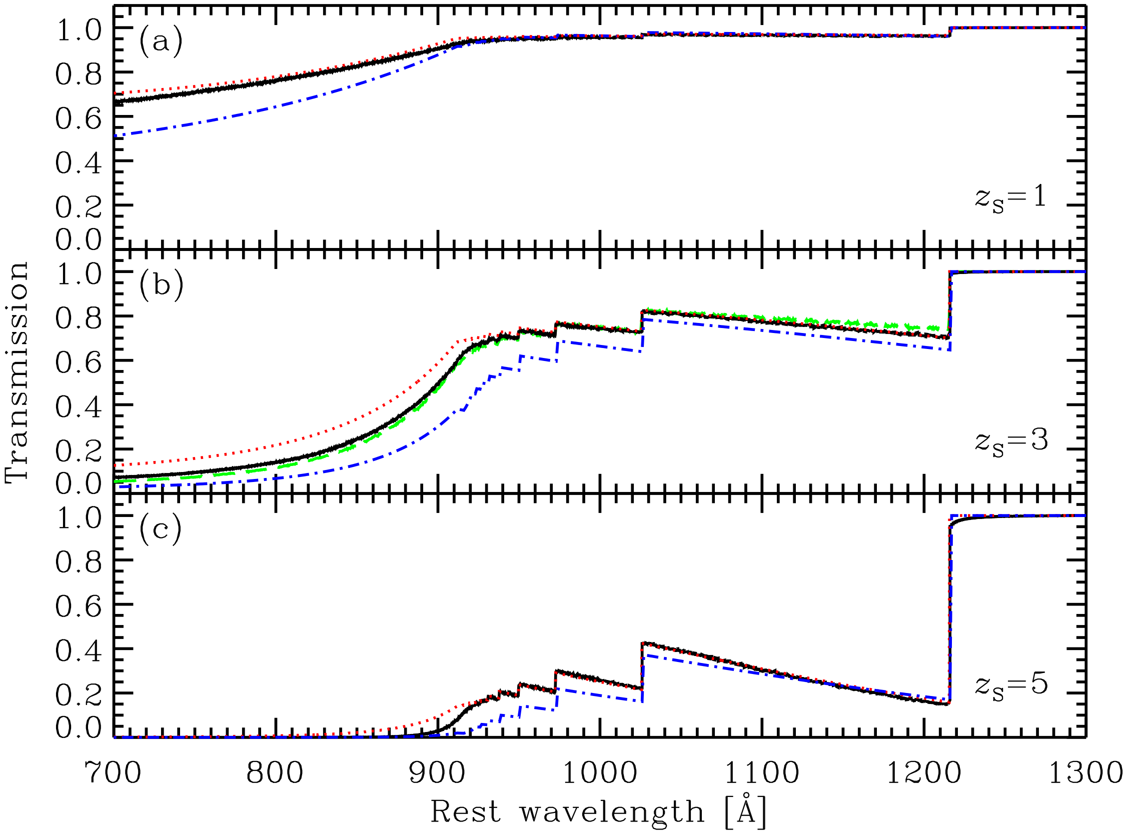

Figure 6. Average IGM transmissions. The horizontal axis is the wavelength in the source rest-frame. The source redshifts are noted in the panels. The solid lines are our Monte Carlo results; 10,000 lines of sight are averaged in each panel. The dot-dashed lines are the mean transmission models of Madau (1995). The dotted lines are the mean transmission models of Meiksin (2006) but the updated version. The dashed line in the panel (c) is the average transmission of the Monte Carlo simulation by Bershady et al. (1999) (MC-Kim model).

panel. Thus, statistical variations are suppressed in a very small level. The dashed line in the panel (b) is the Monte Carlo model by Bershady et al. (1999) (MC-Kim model). Although the adopted distribution function of the absorbers is different from ours, we find a good agreement between Bershady et al. (1999) and us for the source redshift $z_S = 3$. This is caused by a coincidence of the number density of the absorbers around $z = 3$ in our model with that in their model. For example, the coincidence of the number of LLSs around $z = 3$ in our model with that in their model shown in Figure 3 makes a very good agreement of both transmissions below the Lyman limit. However, we may expect that some differences appear for other redshifts because of differences of the number density of the absorbers in other redshifts.

As the dotted lines in Figure 6, we show the mean transmission models by Meiksin (2006). This is not the original version but the updated one where the treatment of the Lyman continuum absorption by the LAF was revised (A. Meiksin, private communication). The agreement between the updated Meiksin (2006) and us is excellent for all the redshift in the Lyman series regime. In the Lyman continuum regime, our simulation shows smaller transmissions than those of Meiksin (2006). This is because the number of LLSs in our model is almost always larger than that in Meiksin (2006) (i.e. the regression line by Stengler-Larrea et al. 1995, see Figure 3). For example, around $z = 3$, the number of LLSs in Meiksin (2006) is about two-thirds of ours and that of Sargent et al. (1989) which is assumed in Bershady et al. (1999), so that the transmission of Meiksin (2006) is larger than ours and Bershady et al. (1999) at $z_{\rm S} = 3$ (panel [b]).

The dot-dashed lines in Figure 6 are the mean transmission models by Madau (1995). We find that Madau (1995) model almost always shows smaller transmissions than recent models. Madau (1995) calculates the Lyman series regime from the equivalent width distribution of the LAF and the Lyman continuum regime from the column density distribution of the LAF and LLSs. Bershady et al. (1999) find that the Lyman series transmissions based on the equivalent width distribution of Madau (1995) are smaller than those based on the column density distribution of Madau (1995), and that the transmissions increase further if the Doppler parameter b distribution is taken into account, while Madau (1995) assumed a constant $b = 35$ km s^{-1}. Tepper-García & Fritze (2008) recently reproduces the Lyman α depression $D_{\rm A}$ for $0 < z < 6$ by their Monte Carlo simulation with the column density distribution of Madau (1995) not the equivalent width distribution, and their model is equivalent with that of Bershady et al. (1999) (but MC-NH model not MC-Kim model shown in Fig. 6). The smaller transmissions of Madau (1995) in the Lyman continuum regime for $z_{\rm S} = 1$ (panel [a]) are probably caused by the larger number of LLSs of Sargent et al. (1989) than ours (see Fig. 3).

4.2 Lyman series and Lyman continuum transmissions

Figure 7 shows transmissions averaged over the wavelength ranges blue-ward of Lyman α, β, and γ lines in the source rest-frame as a function of the source redshift. The case blue-ward of Lyman β line includes both of Lyman α absorption and Lyman β absorption. The case blue-ward of Lyman γ line includes Lyman γ absorption as well as Lyman α and β absorptions. Note that the transmissions shown in Figure 7 are wavelength-averaged ones, but those in Figure 6 are averaged over lines of sight. The filled circles with error-bars denote the median and the central 68% range in the distribution of the wavelength-averaged transmissions of 10,000 lines of sight for each source redshift. In the panels, we also show observational

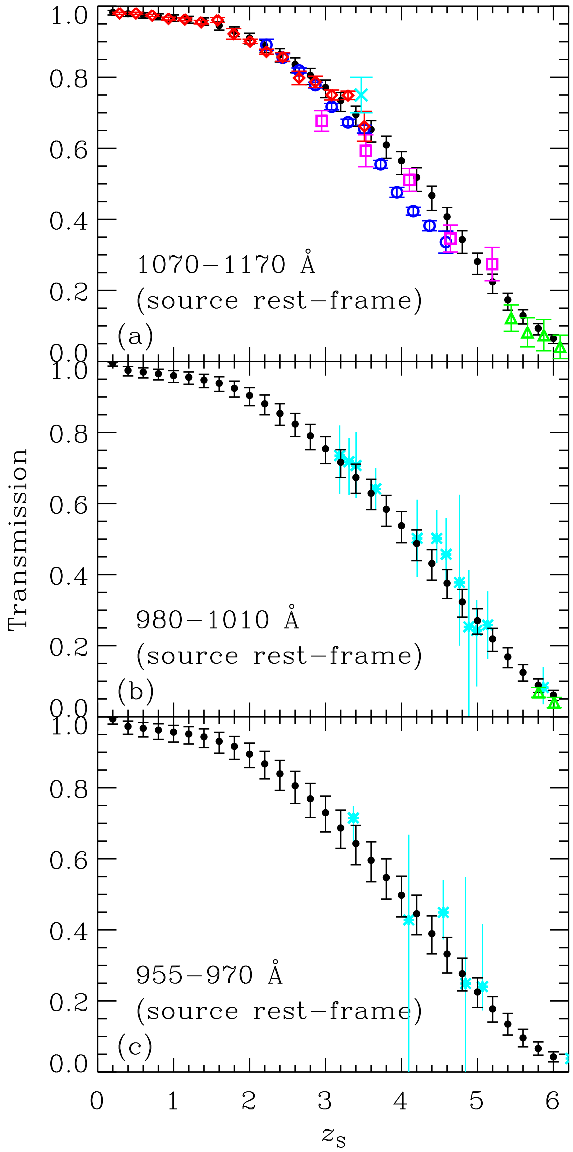

Figure 7. Transmissions averaged over the wavelength ranges blue-ward of Lyα (1070–1170 Å; [a]), Lyβ (980–1010 Å; [b]), and Lyγ (955–970 Å: [c]) in the source rest-frame. The horizontal axis is the source redshift. The filled circles with vertical error-bars are median and the central 68% range of the wavelength-averaged transmissions for 10,000 lines of sight generated in our Monte Carlo simulation. The open diamonds, circles, triangles, and asterisks are taken from Kirkman et al. (2007), Faucher-Giguère et al. (2008), Fan et al. (2006), and Songaila (2004), respectively. The open squares are the data obtained from Tepper-García & Fritze (2008) but binned and corrected for the metal absorptions (the method by Tytler et al. 2004) by us. The cross mark is the estimation by us based on the observations by Steidel et al. (2001) (see appendix A).

estimations for comparisons. We find an excellent agreement between our simulation and the observed data although a dispersion of the observed data is still found at $z_S \gtrsim 3$. This excellent agreement ensures the validity of our model for the Lyman series absorption.

There are small upwards shifts of the filled circles (our model predictions) at the source redshift $z_S = 0.2$ relative to those at $z_S \geqslant 0.4$ in the panels (b) and (c). These features are due to the lack of the Lyman α absorptions in the considering wavelength ranges. For example, to absorb the radiation of the Lyman β range (980–1010 Å) of $z_S = 0.2$ by Lyman

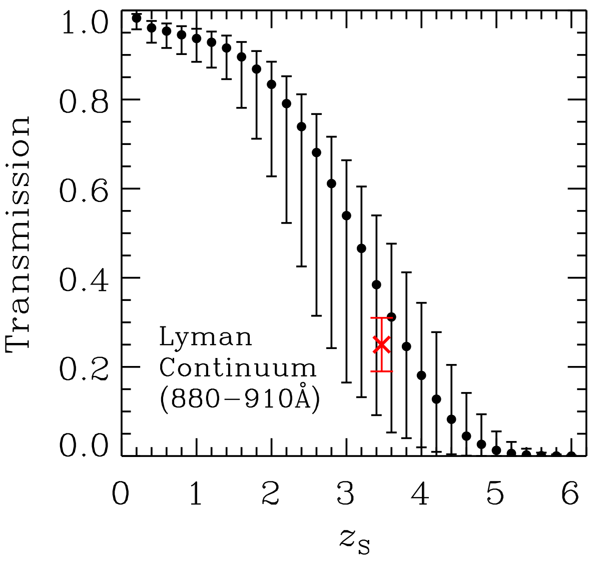

Figure 8. Transmissions averaged over the wavelength range of the Lyman continuum (880–910 Å) in the source rest-frame. The horizontal axis is the source redshift. The filled circles and vertical error-bars are median and the central 68% range of the wavelength-averaged transmissions for 10,000 lines of sight generated in our Monte Carlo simulation. The cross mark is the estimation by us based on the composite spectrum of 15 QSOs at $\langle z\rangle = 3.47$ by Steidel et al. (2001) (see appendix A).

α line, we would need absorbers with negative redshift. Since we consider the absorbers only at a positive redshift, the transmission in the Lyman β range shows such a small jump between $z_S = 0.2$ and 0.4. The same is true for the Lyman γ transmission.

Figure 8 shows transmissions averaged over the wavelength range of the Lyman continuum in the source rest-frame as a function of the source redshift. This wavelength-averaged transmissions include all the Lyman series absorption and the Lyman continuum absorption. The filled circles and error-bars are the median and the central 68% range of the distribution of the wavelength-averaged transmissions of 10,000 lines of sight for each source redshift. We first find that the dispersion is quite larger than those of Lyman series wavelengths shown in Figure 7. The stochastic nature of the Lyman continuum absorption results in such a large variance. We also show the observed estimation of the Lyman continuum transmission by Steidel et al. (2001) in the figure. This is based on the composite spectrum of 15 QSOs at $\langle z\rangle = 3.47$ (see appendix A for details). The value is compatible with our Monte Carlo simulation although it is somewhat smaller than the median of our simulation. In order to examine the validity of our model for the Lyman continuum absorption, we need other independent observational estimations of the Lyman continuum transmissions, which seems quite rare in the literature at the moment. We would encourage observational measurements of the Lyman continuum transmissions. The small jump in our model between the source redshift $z_S = 0.2$ and 0.4 because of the same reason of Figure 7 (b) and (c).

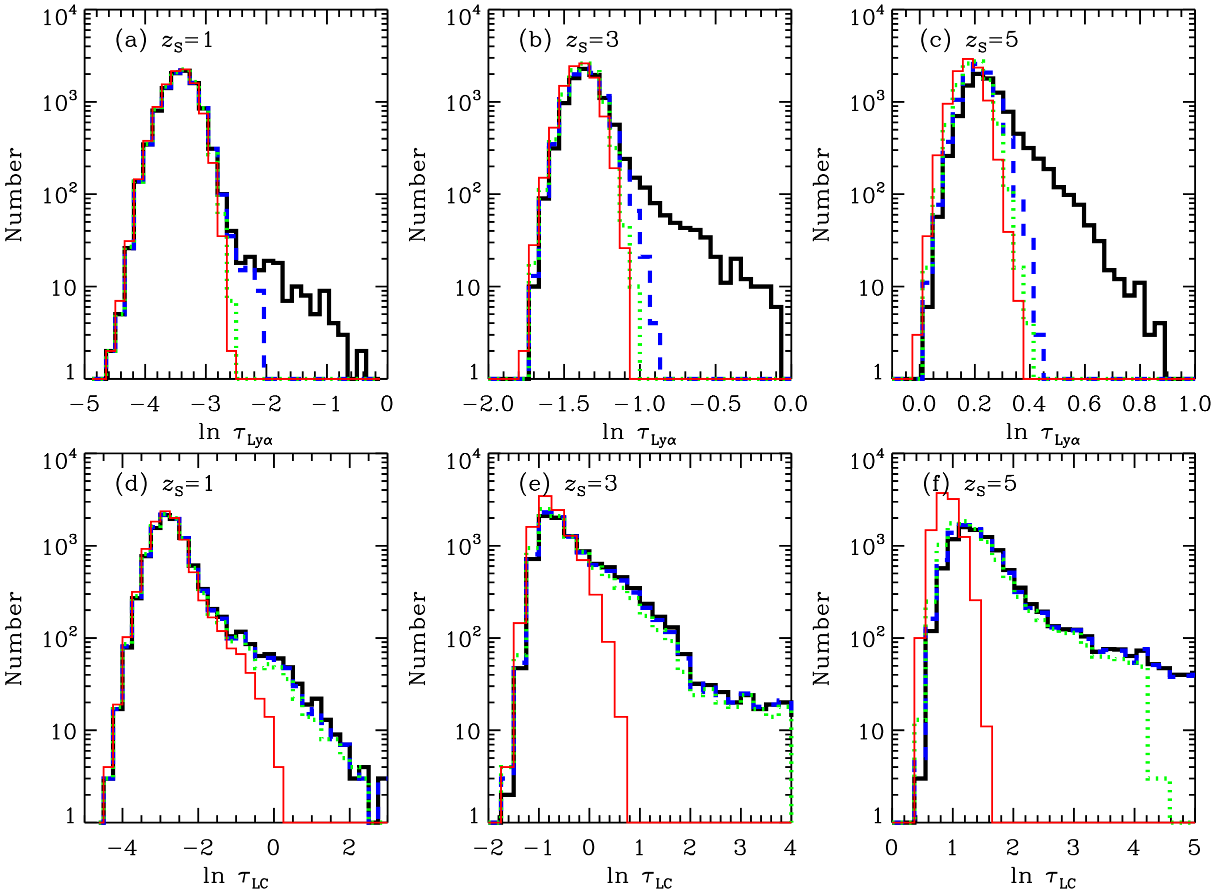

Figure 9. Histograms of the logarithm of effective optical depths in the wavelength ranges blue-ward of Lyα (1070–1170 Å; [a]–[c]) and of the Lyman limit (880–910 Å; [d]–[f]) in the source rest-frame. The source redshifts are noted in the panels. The thin solid histograms are the cases with only the LAF contribution (i.e. $\log_{10} N_{\rm HI}/{\rm cm}^{-2} < 17.2$). The dotted histograms are the cases with the LAF and LLSs ($\log_{10} N_{\rm HI}/{\rm cm}^{-2} < 19.0$). The dashed histograms are the cases without DLAs ($\log_{10} N_{\rm HI}/{\rm cm}^{-2} < 20.3$). The thick solid histograms are the cases with all types of absorbers. Each histogram consists of 10,000 lines of sight.

4.3 Opacity distribution functions

Figure 9 shows histograms of the logarithm of effective optical depths ($\ln \tau_{\rm eff}$) corresponding to the wavelength-averaged transmission shown in Figures 7 and 8 (i.e. $\tau_{\rm eff} \equiv -\ln\langle T\rangle$), of the Lyman α regime (the panels [a]–[c]) and of the Lyman continuum regime (the panels [d]–[f]) for three source redshifts. The thick solid histograms are the cases where all types of absorbers are taken into account. On the other hand, the dashed histograms are the cases without DLAs, the dotted histograms are the cases without DLAs and sub-DLAs, and the thin solid histograms are the cases of only the LAF contribution.

The histograms of $\ln \tau_{{\rm Ly}\alpha}$ of all absorbers (thick solid ones in panels [a]–[c]) show a broad tail towards large opacity, whereas the histograms without DLAs do not show such prominent tails. Thus, we conclude that these tails are mainly caused by DLAs ($N_{\rm HI} > 2 \times 10^{20}$). Since the number density of DLAs increases along the redshift as shown in Figure 2, these tails become more significant for higher redshifts. The $z_{\rm S}=5$ histogram of all absorbers seems largely modulated by the tail, whereas the fraction of lines of sight with $\ln\tau_{\rm Ly\alpha}>-1.0$ for $z_{\rm S}=3$ is 5%, and the fraction of lines of sight with $\ln\tau_{\rm Ly\alpha}>-2.5$ for $z_{\rm S}=1$ is 1.4%. We also note that the effect of LLSs and sub-DLAs on $\tau_{\rm Ly\alpha}$ is small. This is already found by Tepper-García & Fritze (2008) with their Monte Carlo simulation and explained very well with the curve-of-growth theory. Since they did not include DLAs in their simulation, however, they could not find the tails found here.

If we exclude DLAs, the histograms of $\ln\tau_{\rm Ly\alpha}$ (thin solid, dotted, and dashed histograms in panels [a]–[c]) seems Gaussian apparently. Note that the Gaussian distribution becomes parabola in the panels since the y-axis is shown in logarithmic scale. Suppose a null hypothesis that the histogram of $\ln\tau_{\rm Ly\alpha}$ is Gaussian in order to examine the Gaussianity quantitatively. Based on the Kolmogorov-Smirnov (K-S) test, we cannot reject the null hypothesis with a significance level of 1% for the cases of only the LAF and of the LAF+LLSs at $z_{\rm S}\geqslant 2$. Thus, the distribution of $\tau_{\rm Ly\alpha}$ for these cases can be regarded as log-normal. For the $z_{\rm S}=1$ cases, however, we can reject the null hypothesis with a significance level of 0.01% by the K-S test. If we include sub-DLAs, Gaussianity of the distribution of $\ln\tau_{\rm Ly\alpha}$ is reduced, but few cases can be regarded as Gaussian (i.e. we cannot reject the null hypothesis with a significance level of 1% for the cases).

We also find that the dispersion of $\ln\tau_{\rm Ly\alpha}$ decreases along the redshift. Note that the displayed range of the x-axis becomes narrower as the redshift becomes larger. Such a log-normal behaviour with a decreasing variance in $\ln\tau_{\rm Ly\alpha}$ is found in the observed probability distribution function of the transmitted flux of the QSOs' spectra (Becker, Rauch, & Sargent 2007). On the other hand, the dispersion of transmissions shown in Figure 7 increases from $z=0$ to $z=3$–4 and decreases towards higher redshifts (see also Tepper-García & Fritze 2008). This difference between the transmission distribution and the logarithmic opacity distribution is caused by logarithmic transformations from transmission to logarithmic opacity.

Tepper-García & Fritze (2008) suggest that the distribution of the wavelength-averaged transmission for higher redshifts approaches Gaussian because of the Central Limit Theorem; sum of the contributions of a large number of absorbers. Indeed, the histograms of the wavelength-averaged transmission in the Lyman α regime of only the LAF case and of the LAF+LLSs case in our simulation could be regarded as Gaussian; we cannot reject the Gaussian hypothesis with a significance level of 1% for these cases at $z_{\rm S}\geqslant 3$ based on the

K-S test. However, we also find with the K-S test that the distribution of $\ln\tau_{\rm Ly\alpha}$ is closer to Gaussian than that of the wavelength-averaged Lyman α transmission.

The histograms of $\ln\tau_{\rm LC}$ (Fig. 9 [d]–[f]) show a broad tail towards large opacity. Unlike $\ln\tau_{\rm Ly\alpha}$, these tails are mainly produced by LLSs. Even in the LAF only case, we find such tails. Thus, the histograms of $\ln\tau_{\rm LC}$ are not Gaussian. These tails make the mode of the opacity always smaller than the mean. Thus, we have a large probability having a transmission larger than that expected from the mean opacity model. We will come back to this point in section 5 where we discuss the detectability of the Lyman continuum of distant galaxies. We note that the cut-off at $\ln\tau_{\rm LC}\approx 4$ found in the LAF+LLSs histograms of panels [e] and [f] corresponds to the optical depth for the upper limit of HI column density of LLSs (i.e. $N_{\rm HI}\leqslant 1\times 10^{19}$ cm^{-2} and $\tau_{\rm LC}\leqslant 63$ for a single LLS).

4.4 Estimating Lyman continuum opacity from Lyman α opacity

Can we estimate the Lyman continuum opacity from the Lyman α opacity? If it is possible, we may estimate the former opacity for an individual distant galaxy because we can estimate the latter opacity from the observed rest-frame 1000–1500 Å spectrum individually.

Figure 10 (a) shows the probability distribution in the plane of the logarithms of the effective Lyman α opacity ($\tau_{\rm Ly\alpha}$) and the effective Lyman continuum opacity ($\tau_{\rm LC}$). This is produced by 300,000 sets of ($\tau_{\rm Ly\alpha},\tau_{\rm LC}$): 30 source redshifts (0.2–6.0 with 0.2 interval) times 10,000 lines of sight. Contrary to the note by Shapley et al. (2006) based on their Monte Carlo simulation of the intergalactic absorption, we find a good correlation between $\ln\tau_{\rm Ly\alpha}$ and $\ln\tau_{\rm LC}$; the correlation coefficient is 0.860. Since Shapley et al. (2006) simulated the intergalactic absorption only for a single source redshift $z_{\rm S}=3.06$, the dynamic range of $\tau_{\rm Ly\alpha}$ might be too small for them to find the correlation. Indeed, the probability density for $z_{\rm S}=3$ shown as the dotted contour in Figure 10 (a) is confined in a small range of $\tau_{\rm Ly\alpha}$ and elongated towards large $\tau_{\rm LC}$. Although LLSs mainly control $\tau_{\rm LC}$ and the LAF does $\tau_{\rm Ly\alpha}$, the LAF still has an effect on $\tau_{\rm LC}$. Thus, the correlation between $\tau_{\rm LC}$ and $\tau_{\rm Ly\alpha}$ seems natural. However, we should confirm it observationally in future. Currently, we have one estimate (cross mark in the figure) based on the composite spectrum of 15 QSOs at $\langle z\rangle=3.47$ by Steidel et al. (2001), which is consistent with our prediction.

In Figure 10 (a), we also show the median and the central 68% range of the $\tau_{\rm LC}$ distribution for 12 $\tau_{\rm Ly\alpha}$ bins. Table 2 is the summary of them. Interestingly, we may estimate a

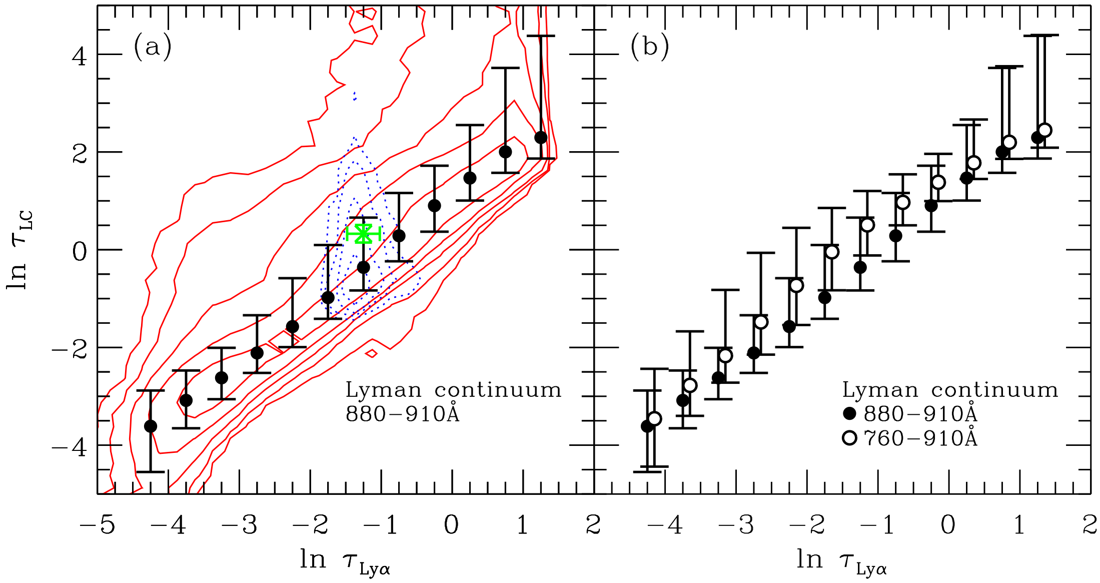

Figure 10. (a) Correlation between the effective optical depths in the wavelength ranges blue-ward of Lyα (1070–1170 Å; horizontal axis) and of the Lyman limit (880–910 Å; vertical axis) in the source rest-frame. The contours show the probability density in this plane and the contour levels are 0.001, 0.003, 0.01, 0.03, and 0.1 from the outside; the solid contour is for $z_{\rm S} = 0.2$–6 and the dotted contour is for $z_{\rm S} = 3$. The filled circles and the error-bars indicate the position of the median and the width of the central 68% range of the distribution in each bin of the horizontal axis (see Table 2). The cross mark is the estimation by us based on the QSO composite spectrum by Steidel et al. (2001) (see appendix A). (b) Difference of the medians and the central 68% ranges for two wavelength ranges of the Lyman continuum; filled symbols are the case of 880–910 Å and open symbols are the case of 760–910 Å. The open symbols are offset to the right by 0.1 dex for graphical clarity.

statistically probable range of $\tau_{\rm LC}$ and Lyman continuum transmission from $\tau_{\rm Ly\alpha}$. We should note that the probable ranges of $\tau_{\rm LC}$ depend on the wavelength range considered. In Figure 10 (b), we show the difference of the medians and the 68% ranges for two cases of the wavelength range in the Lyman continuum: filled symbols are the case of 880–910 Å and open symbols are the case of 760–910 Å. For a wider wavelength case, we expect a larger optical depth (i.e. smaller transmission) because of a larger probability having a LLS in the considering wavelength range. Thus, we should care the wavelength range to estimate $\tau_{\rm LC}$ from $\tau_{\rm Ly\alpha}$. In Table 2, we have taken the wavelength range of 880–910 Å in the source rest-frame.

5 DETECTABILITY OF LYMAN CONTINUUM

Although the observations of the Lyman continuum is very challenging because of the intergalactic absorption as well as the interstellar one, Shapley et al. (2006) did detect the continuum from 2 out of 14 Lyman break galaxies at $z \sim 3$. On the other hand, Malkan, Webb, & Konopackey (2003) and Siana et al. (2007) did not detect the continuum from total 32 star-forming galaxies at $z \sim 1$. Combining these results of direct observations with an indirect estimation from the ionising background intensity, Inoue et al. (2006) sug-

Table 2. Median and central 68% width of the distribution of $\ln\tau_{\rm LC}$ and corresponding Lyman continuum transmission as a function of $\ln\tau_{\rm Ly\alpha}$.

		$\ln\tau_{\rm LC}$			transmission rate	
$\ln\tau_{\rm Ly\alpha}$	median	lower	upper	median	lower	upper
-4.25	-3.61	-4.55	-2.88	0.973	0.945	0.989
-3.75	-3.08	-3.65	-2.47	0.955	0.919	0.974
-3.25	-2.62	-3.06	-2.01	0.930	0.875	0.954
-2.75	-2.11	-2.52	-1.34	0.886	0.770	0.923
-2.25	-1.57	-1.99	-0.58	0.812	0.571	0.872
-1.75	-0.98	-1.41	0.10	0.687	0.331	0.783
-1.25	-0.36	-0.83	0.66	0.498	0.144	0.647
-0.75	0.28	-0.24	1.16	0.266	0.041	0.455
-0.25	0.90	0.37	1.72	0.085	0.003	0.235
0.25	1.47	1.01	2.55	0.013	0.000	0.064
0.75	2.00	1.57	3.72	0.001	0.000	0.008
1.25	2.30	1.87	4.38	0.000	0.000	0.002

The wavelength ranges are 1070–1170 Å for Lyα and 880–910 Å for the Lyman continuum in the source rest-frame.

gested an evolution of the cosmic average escape fraction along the redshift: larger escape fraction at higher redshift on average. Such an evolution scenario of the average escape fraction seems to be supported by a recent cosmological simulation (Razoumov & Sommer-Larsen 2006, 2007). Shapley et al. (2006) showed that some galaxies do have a large escape fraction. If the number of the galaxies with a large escape fraction increases along the redshift, such galaxies may contribute to the cosmic reionisation significantly. Thus, understanding the properties of such galaxies is very interesting. However, any common property in two detected galaxies of Shapley et al. (2006) were not found. We may need much more number of galaxies showing a large escape of the Lyman continuum. Here, we discuss the detectability of such galaxies at $z \geqslant 1$ using the intergalactic transmission presented in the previous section.

The observable flux density of the Lyman continuum is expressed as

$$F_{\rm LC}^{\rm obs} = \mathcal{R}_{\rm esc} F_{\rm UV}^{\rm obs} T_{\rm LC}^{\rm IGM} \,, \tag{11}$$

where $\mathcal{R}_{\rm esc}$ is the escaping flux density ratio of the Lyman continuum to the non-ionising ultraviolet introduced by Inoue et al. (2006), $F_{\rm UV}^{\rm obs}$ is the observed non-ionising ultraviolet flux density, and $T_{\rm LC}^{\rm IGM}$ is the intergalactic transmission of the Lyman continuum. We may use the escape ratio $\mathcal{R}_{\rm esc}$ as a proxy of the absolute escape fraction because they are the same order usually (Inoue et al. 2006). Estimating the absolute escape fraction is difficult in general because we need the dust attenuation correction and the intrinsic spectrum, while $\mathcal{R}_{\rm esc}$ is just the observed flux density ratio corrected for the IGM opacity (see Inoue et al. 2006 for details).

Suppose an observation in the Lyman continuum of distant galaxies with a limiting flux

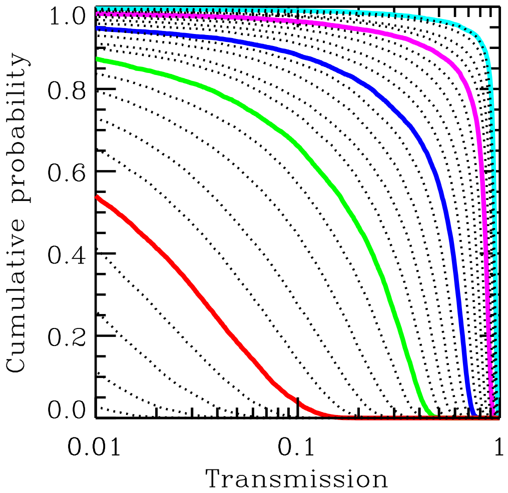

Figure 11. Probability of having a line of sight with a transmission averaged over the Lyman continuum (880–910 Å) in the source rest-frame larger than the value indicated in the horizontal axis. The lines from right to left are the cases of the source redshift from 1.0 to 5.8 with the redshift interval of 0.2. The cases of the source redshift of 1, 2, 3, 4, and 5 are indicated as the thick solid lines.

density $F_{\rm LC}^{\rm lim}$. In other words, we can detect a galaxy with its flux density in the Lyman continuum of $F_{\rm LC}^{\rm obs} \geqslant F_{\rm LC}^{\rm lim}$ with an enough significance. In this case, the IGM transmission towards the galaxy must satisfy

$$T_{\rm LC}^{\rm IGM} \geqslant T_{\rm LC}^{\rm lim} \equiv \frac{F_{\rm LC}^{\rm lim}}{\mathcal{R}_{\rm esc} F_{\rm UV}^{\rm obs}} \,. \qquad (12)$$

The quantity $T_{\rm LC}^{\rm lim}$ means the minimum IGM transmission for a galaxy to be detected by an observation. Thus, the detectable probability of a galaxy is the probability that we have a transmission equal to or larger than $T_{\rm LC}^{\rm lim}$. The detectable probability becomes larger for a fainter $F_{\rm LC}^{\rm lim}$ (i.e. deeper observation), a larger $\mathcal{R}_{\rm esc}$ (i.e. larger escape fraction), or a brighter $F_{\rm UV}^{\rm obs}$ (i.e. more luminous object).

Figure 11 shows the probability of lines of sight with a Lyman continuum transmission $T_{\rm LC}^{\rm IGM}$ larger than the value indicated in the horizontal axis. This is just a cumulative probability calculated from 10,000 transmissions produced by our Monte Carlo simulation for each source redshift $z_{\rm S}$. We show 5 cases of $z_{\rm S} = 1$–5 as the thick solid lines. The case of $z_{\rm S} = 6$ is always zero probability in the range of the horizontal axis shown in the figure. We expect that the fraction of lines of sight not opaque against the Lyman continuum from $z_{\rm S} = 3$ (i.e. $T_{\rm LC}^{\rm IGM} > 0.37$ for $\tau_{\rm LC} < 1$) is 70%, and the fraction even for $z_{\rm S} = 3.8$ is 25%.

Table 3 is a summary of the expected detectable probability (%) with the assumption of $\mathcal{R}_{\rm esc} = 0.3$ which is estimated from the two detections of Shapley et al. (2006). When observing the Lyman continuum of 880–910 Å in the source rest-frame, we find that 70–

Table 3. Detectable probability of a galaxy with a large escape fraction.

	$m_{\rm LC}^{\rm limit}-m_{\rm UV}^{\rm obs}$ (AB)						
$z_{\rm S}$	1.5	2.0	2.5	3.0	3.5	4.0	4.5
1.0	90	96	98	99	99	99	99
2.0	49	88	92	94	96	97	97
3.0	0	52	73	81	86	89	91
4.0	0	0	19	45	59	70	76
5.0	0	0	0	0	1	7	17

The detectable probability (%) of a galaxy with a large escape ratio of $\mathcal{R}_{\rm esc}=0.3$ at the redshift $z_{\rm S}=1$–5 when observing the wavelength range of 880–910 Å in the source rest-frame. Seven cases of the limiting magnitude of the Lyman continuum observation are shown: $m_{\rm LC}^{\rm limit}=m_{\rm UV}^{\rm obs}+1.5$, 2.0, 2.5, 3.0, 3.5, 4.0, and 4.5, where $m_{\rm UV}^{\rm obs}$ is the observed magnitude in the non-ionising ultraviolet (∼1500 Å in the rest-frame) of the galaxy. We expect a larger probability for a deeper observation (i.e. larger $m_{\rm LC}^{\rm limit}$) or a more luminous object (i.e. smaller $m_{\rm UV}^{\rm obs}$). Note that the detectable probability depends on the observing wavelength range (see text).

80% galaxies with a large escape fraction of $\mathcal{R}_{\rm esc}=0.3$ are detectable for $z_{\rm S}=3$ and 20–45% galaxies are detectable even for $z_{\rm S}=4$ if the objects are 24.5 AB in UV and the limiting magnitude of the Lyman continuum is 27.0–27.5 AB. In the observations of Shapley et al. (2006), the limiting magnitude of the Lyman continuum and the average observed UV magnitude are 27.56 AB and 23.92 AB, respectively, and the average redshift is 3.06; the detectable probability of a galaxy with $\mathcal{R}_{\rm esc}=0.3$ in their sample is about 90%. Since Shapley et al. (2006) detected 2 out of 14 galaxies, therefore, we expect that the fraction of the galaxies with $\mathcal{R}_{\rm esc}=0.3$ is about 16% in their sample. This suggests that there is a large variance of the escape fraction at $z\sim3$, which is very interesting and whose origin should be understood in the context of the galaxy evolution in future.

We note that the detectable probability in Table 3 may be the most optimistic case because the probability depends on the observing wavelength range. If we observe a wider wavelength range, the probability of having a LLS in the corresponding redshift range increases, then, the transmission and the detectable probability decreases. In addition, if we observe a wavelength range far from the Lyman limit (e.g., ~ 700 Å), the probability affected by a LLS also increases, then, the detectable probability decreases (see also Figs. 4-6 and 10). Therefore, we should take into account the observing wavelength range properly when estimating the detectable probability for future observations.

6 CONCLUSIONS

Motivated by recent attempts for determining the escape fraction of the Lyman continuum from distant galaxies, we have made a Monte Carlo simulation of the intergalactic absorption in order to model the Lyman continuum absorption properly. For this simulation, we have derived an empirical distribution function of the intergalactic absorbers, Lyman α forest (LAF), Lyman limit systems (LLSs), and damped Lyman α systems (DLAs), from the observed statistics of the absorbers. In the distribution function of the absorbers, we have assumed a single functional form of the redshift distribution for all types of the absorbers, while the previous models of the intergalactic absorption assumed two different functional forms for the LAF and LLSs (and DLA).

The transmission functions obtained from our simulation are very consistent with the previous models except for Madau (1995) which predicts smaller transmissions than others. The Lyman series transmissions by our simulation excellently agree with the observational data, which ensures validity of our model. We have predicted the Lyman continuum transmissions as a function of the source redshift. Although observational estimates of the Lyman continuum transmission are quite rare in the literature, one observational estimate based on Steidel et al. (2001) is consistent with our prediction.

The distribution function of the Lyman α opacity for a source redshift seems log-normal with a tail towards large opacities. This tail is produced by DLAs. Since the number density of DLAs increases along the redshift, the significance of the tail in the distribution function increases. As found by Tepper-García & Fritze (2008), we also find that the effect of LLSs on the Lyman α opacity is small. Along the source redshift, the mean of the log-normal part increases but the variance decreases. These features are found in recent observations.

The distribution function of the Lyman continuum opacity shows a very broad tail towards a large opacity which is produced by LLSs. Unlike the Lyman α opacity, the effect of DLAs on the Lyman continuum opacity is small. Rarity of LLSs controlling the Lyman continuum opacity provides us with a chance to have a clean line of sight for $z \sim 4$; the probability of a clean (i.e. optical depth less than unity) line of sight at 900 Å in the source rest-frame is about 70% for the source redshift $z \sim 3$ and about 20% for $z \sim 4$.

A good correlation between the Lyman α opacity and the Lyman continuum one is found although Shapley et al. (2006) noted no correlation in their simulation. This may be because a small dynamic range of the Lyman α opacity in their simulation. Based on the correlation we find, we may predict a statistically probable range of the Lyman continuum opacity as a function of the Lyman α opacity. This may be useful to estimate the Lyman continuum opacity from the Lyman α one for individual galaxy.

Finally, we have predicted the detectable probability of a galaxy with a large escape fraction of the Lyman continuum based on our simulation. For example, the detectable probability is 86% when the limiting magnitude of the Lyman continuum observations is 3.5 AB deeper than the non-ionising ultraviolet magnitude of the sample galaxy with an escape ratio $\mathcal{R}_{\rm esc} = 0.3$ at $z = 3$. The small number fraction of the galaxies detected in the Lyman continuum by Shapley et al. (2006) (2 out of 14 sample galaxies) suggests a large variance of the escape fraction at $z = 3$. This should be understood in the context of the galaxy evolution in future.

ACKNOWLEDGMENTS

We would like to thank J.-M. Deharveng for stimulating discussions, C. Péroux for some comments on the distribution function of the intergalactic absorbers, A. Meiksin for giving his updated absorption model and discussing several points on modelling, M. Matsumoto for distributing C-codes of the "Mersenne Twister" on his web page, and the referee, T. Tepper-García for interesting discussions and useful comments. AKI and II are supported by Grand-in-Aid for Young Scientists (B).

REFERENCES

Bahcall, J. N., Peebles, P. J. E., 1969, ApJ, 156, L7

Becker, G. D., Rauch, M., Sargent, W. L. W., 2007, ApJ, 662, 72

Bershady, M. A., Charlton, J. C., Geoffroy, J. M., 1999, ApJ, 518, 103

Davé, R., Hernquist, L., Katz, N., Weinberg, D. H., 1999, ApJ, 511, 521

Fan, X., Strauss, M. A., Becker, R. H., White, R. L., Gunn, J. E., Knapp, G. R., Richards, G. T., et al., 2006, AJ, 132, 117

Faucher-Giguère, C.-A., Prochaska, J. X., Lidz, A., Hernquist, L., Zaldarriaga, M., 2008, ApJ, submitted, (arXiv:0709.2382)

Ferland, G. J., 1996, in Hazy, A Brief Introduction to Cloudy 90, University of Kentucky Internal Report

Giallongo, E., Cristiani, S., 1990, MNRAS, 247, 696

Giallongo, E., Cristiani, S., D'Odorico, S., Fontana, A., 2002, ApJ, 568, L9

Gunn, J. E., Peterson, B. A., 1965, ApJ, 142, 1633

Hui, L., Rutledge, R. E., 1999, ApJ, 517, 541

Inoue, A. K., Iwata, I., Deharveng, J.-M., Buat, V., & Burgarella, D., 2005, A&A, 435, 471

Inoue, A. K., Iwata, I., Deharveng, J.-M., 2006, MNRAS, 371, L1

Janknecht, E., Reimers, D., Lopez, S., Tytler, D., 2006, A&A, 458, 427

Kawaguchi, T., Shimura, T., Mineshige, S. 2001, ApJ, 546, 966

Kim, T.-S., Cristiani, S., D'Odorico, S., 2001, A&A, 373, 757

Kim, T.-S., Carswell, R. F., Cristiani, S., D'Odorico, S., Giallongo, E., 2002, MNRAS, 335, 555

Kirkman, D., Tytler, D., Lubin, D., Charlton, J., 2007, MNRAS, 376, 1227

Madau, P., 1995, ApJ, 441, 18

Malkan, M., Webb, W., Konopacky, Q., 2003, ApJ, 598, 878

Matsumoto, M., Nishimura, T., 1998, ACM Transactions on Modeling and Computer Simulation, 8, 3

Meiksin, A., 2006, MNRAS, 365, 807

Møller, P., Jakobsen, P., 1990, A&A, 228, 299

Murdoch, H. S., Hunstead, R. W., Pettini, M., Blades, J. C., 1986, ApJ, 309, 19

O'Meara, J. M., Prochaska, J. X., Burles, S., Prochter, G., Bernstein, R. A., Burgess, K. M., 2007, ApJ, 656, 666

Osterbrock, D. P., 1989, in Astrophysics of gaseous nebulae and active galactic nuclei, University Science Books, Mill Valley, CA

Ostriker, J. P., Bajtlik, S., Duncan, R. C., 1988, ApJ, 327, L35

Paresce, F., McKee, C. F., Bowyer, S., 1980, ApJ, 240, 387

Péroux, C., McMahon, R. G., Storrie-Lombardi, L. J., & Irwin, M. J., 2003, MNRAS, 346, 1103

Péroux, C., Dessauges-Zavadsky, M., D'Odorico, S., Kim, T.-S., McMahon, R. G., 2005, MNRAS, 363, 479

Prochaska, J. X., Herbert-Fort, S., Wolfe, A. M., 2005, ApJ, 635, 123

Rao, S. M., Turnshek, D. A., Nestor, D. B., 2006, ApJ, 636, 610

Rauch, M., 1998, ARA&A, 36, 267

Razoumov, A., Sommer-Larsen, J., 2006, ApJ, 651, L89

Razoumov, A., Sommer-Larsen, J., 2007, ApJ, 668, 674

Sargent, W. L. W., Steidel, C. C., Boksenberg, A., 1989, ApJS, 69, 703

Scott, J. E., Kriss, G. A., Brotherton, M., Green, R. F., Hutchings, J., Shull, J. M., Zheng, W. 2004, ApJ, 615, 135

Shang, Z.,; Brotherton, M. S., Green, R. F., Kriss, G. A., Scott, J., Quijano, J. K., Blaes, O., Hubeny, I., et al., 2005, ApJ, 619, 41

Shapley, A. E., Steidel, C. C., Pettini, M., Adelberger, K. L., Erb, D. K., 2006, ApJ, 651, 688

Siana, B., Teplitz, H. I., Colbert, J., Ferguson, H. C., Dickinson, M., Brown, T. M., Conselice, C. J., de Mello, D. F., et al., 2007, ApJ, 668, 62

Songaila, A., 2004, AJ, 127, 2598

Steidel, C. C., Pettini, M., & Adelberger, K. L., 2001, ApJ, 546, 665

Stengler-Larrea, E. A., Boksenberg, A., Steidel, C. C., Sargent, W. L. W., Bahcall, J. N., Bergeron, J., Hartig, G. F., Jannuzi, B. T., et al., 1995, ApJ, 444, 64

Telfer, R. C., Zheng, W., Kriss, G. A., Davidsen, A. F., 2002, ApJ, 565, 773

Tepper-García, T., 2006, MNRAS, 369, 2025

Tepper-García, T., Fritze, U., 2008, MNRAS, 383, 1671

Tytler, D., 1987, ApJ, 321, 49

Tytler, D., Kirkman, D., O'Meara, J. M., Suzuki, N., Orin, A., Lubin, D., Pascal, P., Jena, T., 2004, ApJ, 617, 1

Weymann, R. J., Jannuzi, B. T., Lu, L., et al., 1998, ApJ, 506, 1

Wiese, W. L., Smith, M. W., & Glennon, B. M., 1966, Atomic transition probabilities, 1, US Department of Commerce, National Buereau of Standards, Washington

Zheng, W., Kriss, G. A., Telfer, R. C., Grimes, J. P., Davidsen, A. F., 1997, ApJ, 475, 469

Zuo, L., 1993, A&A, 278, 343

APPENDIX A: LYMAN α AND LYMAN CONTINUUM TRANSMISSIONS BASED ON QSO COMPOSITE SPECTRUM BY STEIDEL ET AL. (2001)

We describe the method for estimating the transmissions in the Lyman α and the Lyman continuum ranges based on the composite spectrum of QSOs by Steidel et al. (2001). The method is essentially same as that used in Steidel et al. (2001). However, we assume a different intrinsic spectrum of QSOs based on the recent observations. The obtained transmissions are plotted in Figures 7, 8, and 10.

The wavelength ranges of the Lyman α and the Lyman continuum transmissions in Figures 7, 8, and 10 are 1070–1170 Å and 880–910 Å, respectively, in the source rest-frame. We take 1100 Å and 900 Å as their representative values. In general, the IGM transmission at a wavelength x is defined as $T_x^{\rm IGM} \equiv F_x^{\rm obs}/F_x^{\rm int}$, where $F_x^{\rm obs}$ and $F_x^{\rm int}$ are the observed and the intrinsic flux densities, respectively. The intrinsic flux density can be estimated from the observed flux density at a wavelength free from the IGM absorption, that is, > 1216 Å, if we assume an intrinsic spectrum. When we assume the reference wavelength of 1500 Å, the Lyman α and the Lyman continuum transmissions are

$$T_{\rm Ly\alpha}^{\rm IGM} = \frac{(F_{1100}/F_{1500})_{\rm obs}}{(F_{1100}/F_{1500})_{\rm int}}\,, \tag{A1}$$

and

$$T_{\rm LC}^{\rm IGM} = \frac{(F_{900}/F_{1500})_{\rm obs}}{(F_{900}/F_{1500})_{\rm int}}\,. \tag{A2}$$

We take the observed flux densities from the composite spectrum of QSOs by Steidel et al. (2001). The sample consists of 15 QSOs at $\langle z \rangle = 3.47 \pm 0.14$. The QSO composite spectrum is constructed in order to compare the composite spectrum of LBGs from which Steidel et al. (2001) detected the Lyman continuum of the sample LBGs. From Table 2 in Steidel et al. (2001), we have $F_{1100}^{\rm obs} = 1.86 \pm 0.02$ and $F_{900}^{\rm obs} = 0.50 \pm 0.03$ in the arbitrary unit of the flux density (per Hz). We obtain $F_{1500}^{\rm obs} = 3.4$ from their value of $(F_{1500}/F_{900})_{\rm obs} = 6.8 \pm 0.4$.

The intrinsic spectrum of QSOs is the largest source of the error in this estimation. The spectra of QSOs can be fit by a composite of power-laws. We here discuss the indices under the power-law assumption: $F_\nu \propto \nu^\alpha$. The index in the extreme-ultraviolet (including the Lyman continuum) is still controversial. Telfer et al. (2002) obtained $\alpha(500 - 1200 \text{ Å}) = -1.76 \pm 0.12$ from 184 QSOs at $z \sim 1$ (see also Zheng et al. 1997). On the other hand, Scott et al. (2004) obtained $\alpha(630 - 1155 \text{ Å}) = -0.56^{+0.38}_{-0.28}$ from 85 AGNs at $z \sim 0.2$ (see also Shang et al. 2005). This contrast may be due to an evolution of the spectrum along the redshift and the luminosity (Scott et al. 2004), and also there may be the difficulty of the correction for the IGM absorption. We here assume two possible indices of $\alpha(< 1100 \text{ Å}) = -1.8 \pm 0.1$ and -0.6 ± 0.3. For longer wavelength, Zheng et al. (1997) obtained $\alpha(1050 - 2200 \text{ Å}) = -0.99 \pm 0.05$. We here adopt $\alpha(> 1100 \text{ Å}) = -1.0 \pm 0.2$, taking into account a large variance of the indices among QSOs (e.g., Shang et al. 2005). Therefore, the intrinsic ratios of the flux densities adopted here are $(F_{1100}/F_{1500})_{\rm int} = 0.73 \pm 0.05$, and $(F_{900}/F_{1500})_{\rm int} = 0.54 \pm 0.04$ or 0.69 ± 0.11.

The observed ratios of the flux densities measured in the composite spectrum of QSOs at $\langle z \rangle = 3.47$ by Steidel et al. (2001) and the intrinsic ratios described above result in $T_{\rm Ly\alpha}^{\rm IGM} = 0.75 \pm 0.05$, and $T_{\rm LC}^{\rm IGM} = 0.28 \pm 0.03$ or 0.22 ± 0.04. Finally, we summarise the Lyman continuum transmission as $T_{\rm LC}^{\rm IGM} = 0.25 \pm 0.06$, where we put the sum of the internal and external errors as an error estimate.

We should note one point here. In the procedure for obtaining the intrinsic spectrum of QSOs, we need the IGM absorption correction. Then, we used the intrinsic spectrum to obtain $T^{\rm IGM}$. Thus, it is like a tautology although the intrinsic spectrum and $T^{\rm IGM}$ are obtained from the different data and the different authors. However, we may consider that the obtained $T^{\rm IGM}$ still have a meaning since we have assumed a wide range of the spectral indices for the intrinsic spectrum. For future measurements of $T^{\rm IGM}$, we may use an independent intrinsic spectrum of QSOs, for example, based on an accretion disk model (e.g., Kawaguchi, Shimura, & Mineshige 2001).